Properties of Electrodeposited CuSCN 2D Layers and Nanowires Influenced by Their Mixed Domain Structure

Dmitry Aldakov,[a,*] Cyril Chappaz-Gillot,[b,c] Raul Salazar,[c] Vincent Delaye,[c] Kathryn A. Welsby,[d] Valentina Ivanova,[c] Peter R. Dunstan[d,*]

[a] CEA, INAC/SPrAM (UMR 5819 CEA-CNRS-Univ. J. Fourier-Grenoble I), Laboratoire d´Électronique Moléculaire, Organique et Hybride, 17 rue des Martyrs, 38054 Grenoble, France

[b] CEA, LITEN/DTS, Laboratoire des Technologies pour les Modules Photovoltaïques, Savoie Technolac, BP 332, 50 Avenue du Lac Léman, 73377 Le Bourget-du-Lac, France

[c] CEA, LETI, MINATEC Campus, 17 rue des Martyrs, 38054 Grenoble, France

[d] Swansea University, Department of Physics, College of Sciences, Centre of Nanohealth, Swansea SA2 8PP, Wales, UK

* dmitry.aldakov@cea.fr, P.R.Dunstan@swansea.ac.uk

Abstract

Electrodeposited copper thiocyanate (CuSCN) thin films and nanowires have been investigated by X-ray photoelectron spectroscopy (XPS), Raman and optical spectroscopy. In addition, atomic force microscopy (AFM), together with scanning and transmission electron microscopy (SEM, TEM), have been employed for structural characterisation. The multiple technique approach allows the correlation between structural, chemical and electrical properties that are unique to the structure of this material. It has been found that CuSCN thin films and nanowires exhibit high crystalline quality with a close to stoichiometric composition. The XPS and Raman spectra suggest that the thiocyanate ion is bound to copper mainly through its S-end, with approximately 12-14 % bound via the N-end.

The applied absorption spectroscopy (Tauc and Urbach plots) points towards the possible coexistence of two large band gaps for the electrodeposited CuSCN. While its interpretation may be problematic from a purely physical perspective, we believe that this is a direct consequence of the occurrence of two CuSCN domains identified by XPS and Raman. A

prominent absorption tail is observed that is assigned as either being due to the high concentration of the traps, or a result of coexisting CuSCN domains. This absorption tail should not be an obstacle for the use of the copper thiocyanate in electronic devices, as the traps density could be reduced by annealing. In addition, non-annealed electrodeposited CuSCN thin films and nanowires of this type have recently been integrated into polymer solar cells and high efficiency has been obtained.

Keywords: copper thiocyanate, XPS, Raman, band gap, p-type semiconductor

Introduction

There is a technological need for the development of transparent p-type inorganic semiconductors to be used as hole-transporting materials in different optoelectronic and photovoltaic devices. At the same time, compared to their n-type counterparts, the choice of known p-type materials is much scarcer.[1,2] One of the very promising materials of this kind is copper thiocyanate (CuSCN). It belongs to the family of pseudohalides, *i.e.* molecules composed of a metal cation and a complex anion; which in this case is the thiocyanate ion (SCN^-). It has very good hole transporting properties owing to the smaller effective mass of holes compared to electrons, combined with decent hole mobility of 0.01-0.1 cm^2/Vs.[3,4] Among its key properties we can list its good chemical stability and an excellent optical transparency due to its wide band gap of 3.6-3.9 eV. A variety of methods has been developed for its deposition. Probably the easiest and most wide-spread way to deposit thin films of CuSCN is by dip-, spin-, spray-coating or doctor-blading of commercial material solutions. It is also possible to fabricate CuSCN by successive ionic layer adsorption and reaction (SILAR),[5] chemical bath deposition (CBD)[6] or electrodeposition.[7–10] Due to the interest to one-dimensional nanostructures, which combine high surface area with excellent charge transfer properties, research efforts have been devoted to prepare it in nanowire form.[11,12] Our research group has recently reported an easy and template-free electrodeposition of CuSCN nanowires on various substrates from an aqueous solution at room temperature.[13–15]

CuSCN has already become a popular material in various optoelectronic devices, especially in 3rd generation solar cells. Thus, thin films of copper thiocyanate have been used as hole transporting material in extremely thin absorber (ETA),[16,17] dye-[8,18–21] or quantum dot

sensitized,[22] and organic solar cells.[15] Recently, its application in transparent thin film transistors[3,4] and UV-photodetectors[23] has been also demonstrated.

Despite numerous advantages and applications of copper thiocyanate, this material remains surprisingly under-investigated. Whilst studies have shed light on the structural and electronic properties of thin films of CuSCN[11,24–26] the properties of the CuSCN nanowires are largely unexplored. Copper thiocyanate properties are very dependent on specific fabrication parameters thus leading to several particularities. First, it can crystallize in two structures: hexagonal or rhombohedral β-phase and the orthorhombic α-phase. Second, the SCN anion is one of the best known examples of ambidentate ions, i.e. those which can exist in two resonance forms, thiocyanate and isothiocyanate.[27] Finally, its p-type conductivity is clearly related to the structural (especially copper deficiency) and surface defects, which add intra-gap levels. Those latter vary significantly depending on the shape and preparation method of CuSCN. All these factors make CuSCN nanowires a very attractive material to be investigated. In the present study an insight into several important properties of electrodeposited CuSCN thin films and nanowires is proposed based upon a multi-technique approach.

Experimental

CuSCN thin films (2D layers) electrodeposition: A 6 mM Cu^{2+} solution was prepared by mixing $CuSO_4 \bullet 5H_2O$ (1 M equivalent) with 10 M equivalent triethanolamine and 5 M equivalent KSCN into deionized water, according to the procedure described in reference [10]. A 2D layer with a thickness around 200 nm was deposited potentiostatically under continuous stirring at potential E = -0.4 V vs saturated calomel electrode (SCE) and passed charge density 25 mC cm^{-2}.

CuSCN nanowires (NW) electrodeposition: A 12 mM Cu^{2+} solution was prepared by mixing $CuSO_4 \bullet 5H_2O$ (1 M equivalent) with 1 M equivalent EDTA and 0.25 M equivalent KSCN into deionized water.[13] The CuSCN nanowires were deposited potentiostatically under continuous stirring at -0.3 V vs SCE for the ITO coated glass substrates. The passed charge density was fixed at 35 mC cm^{-2} for shorter nanowires (around 400 nm long) and at 80 mC cm^{-2} for longer nanowires (around 1.5 μm long).

X-ray Photoelectron Spectroscopy (XPS) measurements were performed on an SSI S-Probe spectrometer from (Euroscan SA) using a monochromatic Al Kα X-ray source (1486.6 eV

photons) at a constant dwell time of 100 ms and pass energy of 50 eV. The core-level signals were obtained at a photoelectron takeoff angle of 35°. The pressure in the analysis chamber was maintained at 10^{-9} mbar or lower. All peaks were adjusted using the C1s peak at 284.6 eV to correct the binding energies for the charge shift. Photoelectrons were detected using a hemispherical analyser, with an angular acceptance of 30° and an energy resolution of 850 meV. Ar^+ etching was performed at a pressure $2x10^{-7}$ mbar with the energy of 1.5 keV. Elemental quantification was performed using CasaXPS software by the analysis of the integral intensity of each core-level line weighed by its corresponding Scofield sensitivity factor available from the internal database of the software.

Raman spectra were obtained using the 532 nm line of a YAG frequency doubled laser coupled to a Renishaw InVia microscope (Renishaw PLC, England) with a 50x objective. Spectra were referenced by the Si 520 cm^{-1} peak. Averages of 5 spectra were obtained at five different locations for each sample at optimised conditions; 0.5 s exposure time of 10 mW laser radiation and 120 acquisitions. The 532 nm line was selected due to very minimal spectral response with a near infra-red laser. Previous studies of bulk metal-thiocyanate confirm low Raman signals at near infra-red unless surface enhanced Raman spectroscopy (SERS) was implemented[28] whereas Raman spectroscopy with the 633 nm line of a HeNe laser has previously been performed without enhancement mechanisms.[29]

Atomic force microscopy (AFM) images were conducted using a JPK instruments Nanowizard II (JPK instruments, Berlin) operated in AC mode. Scanning electron microscopy (SEM) was conducted with an FEI Nova NanoSEM for the surface morphology characterizations. Transmission electron microscopy (TEM) characterization was done with a FEI Tecnai Osiris microscope at 200 kV, an objective aperture was inserted to select the transmitted beam and reveal the crystalline nature of the specimen. The optical transmission properties of the electrodeposited CuSCN layers were determined in the visible-near-infrared wavelength region using a Perkin Elmer Lambda 35 spectrophotometer.

Results and Discussion

Here we present a multiple technique approach in the study of electrodeposited CuSCN nanowires and 2D films. Specifically we investigate short (400 nm) and long (1-1.3 µm) nanowires, and make comparisons with the 200 nm thick 2D layer.

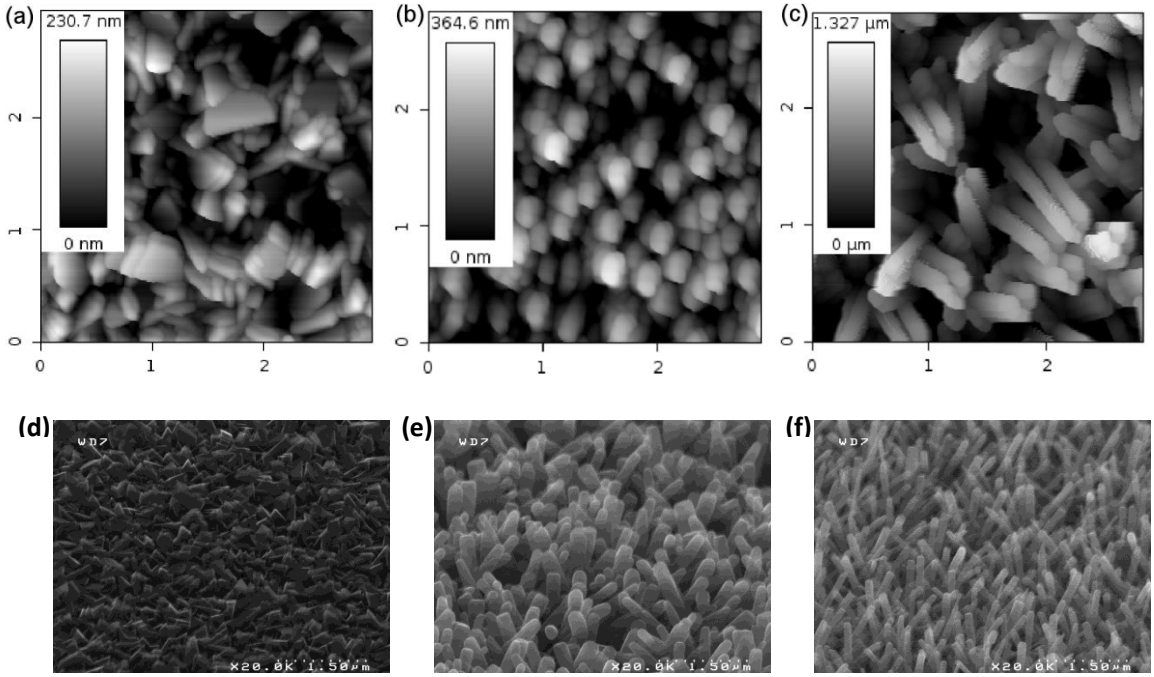

Figure 1. AFM images (a-c) taken with dimensions 3 µm x 3 µm; the corresponding black-to-white height scales are shown individually on each scan. SEM images (d-f) were taken with x 20k magnification. The 2D platelets, 400 µm and 1.4 µm samples are shown in AFM images (a), (b) and (c) respectively and in SEM images (d), (e) and (f) respectively.

Figure 1 presents the topography of the CuSCN thin film and nanowire arrays investigated by atomic force microscopy (AFM) (Figure 1a-c) and scanning electron microscopy (SEM) (Figure 1d-f). Both the AFM and SEM surface scans support the assignment of the nanostructure growth of CuSCN and also confirm the homogeneity of the fabricated samples. Cross-sectional measurements on the AFM scans were used to estimate the diameter of the studied nanowires: for each sample five nanowire feature diameters were recorded with the aim to obtain a mean estimate, results of which are detailed in table 1. For both the short and the long nanowires, the average diameter was found to be approximately 115 nm. The black to white contrast displayed alongside the AFM scan images in figure 1a-c represents the height scale of the AFM scans. This was used to estimate either the mean length of the nanowires grown or the mean thickness of the 2D layer (platelets) deposited. The values found are in a good agreement with SEM cross-section estimates.

Table 1: AFM cross sectional measurements of the three samples allowed for estimations of nanowire diameter for both nanowire samples. The measurement ranges are included to demonstrate its variation over the sample surface. Image contrasts (B/W contrast ratio) from the AFM scans are also stated.

Sample	Diameter, nm	B/W contrast ratio, nm
2D surface	-	231

Short nanowires	117±11	364
Long nanowires	114±15	1327

High resolution TEM analysis of the electrodeposited CuSCN nanowires was carried out in order to investigate their crystalline structure (see Supporting Information). The images confirm a very high crystalline quality of the studied materials. Fourier transform of the TEM images was applied to calculate the spacings between the lattice fringes, which turn out to be constant throughout all the sample zones studied. At the same time, they do not allow to distinguish unambiguously between the alpha and beta phases of the material.

A comprehensive XPS study has been performed on the samples of electrodeposited CuSCN 2D layer and nanowires. The XPS survey spectra shown in figure 2 indicate the presence of the expected elements: copper, sulfur, carbon and nitrogen. The 2D layer spectrum (figure 2a) indicates a trace oxygen contribution, which was probably due to the inevitable presence of surface impurities.

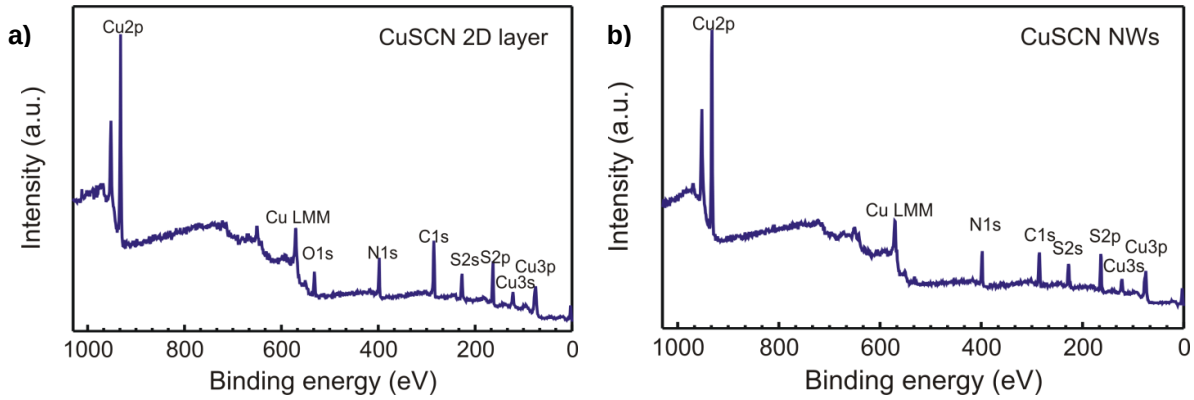

Figure 2. Wide X-ray photoelectron spectra of electrodeposited: a) CuSCN 2D layer and b) CuSCN nanowire array.

In order to get more precise qualitative and quantitative information about the chemical composition and state of the elements, high-resolution spectra of the characteristic regions were recorded and are presented in figure 3 for the 2D CuSCN film. C1s spectral region of a 2D film can be deconvoluted into four peaks. The peak at 284.6 eV, which was used for the calibration of the whole spectrum, is ascribed to the aliphatic carbon sp^3 impurities present on the surface, while the small peak at the highest energy (286.5 eV) corresponds probably also to the adventitious carbon in its oxidized C-OH form. The spectrum is dominated by a peak at 285.7 eV, which is likely the sp-state carbon in its -C≡N form.

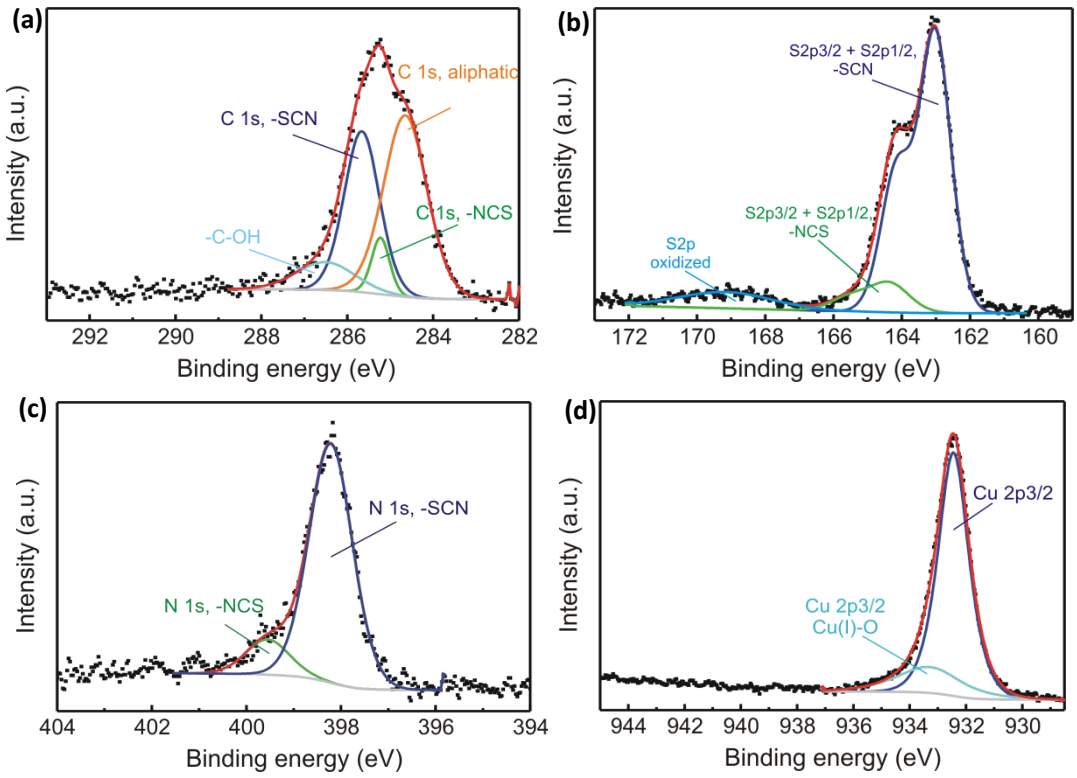

Figure 3. High-resolution XPS spectra for carbon (a), sulfur (b), nitrogen (c) and copper (d) regions for the 2D films of CuSCN.

The spectrum in the sulfur 2p region has been fitted by a series of 3 doublets of S 2p3/2 and S 2p1/2 each. Once again, the spectrum is dominated by a large signal with 2p3/2 peak situated at 163.0 eV, which was ascribed to a sulfur atom in a $^{-}$S-C form. The small peak at 168.8 eV is likely the trace of the oxidized sulphur. The spectrum of N 1s has a major peak at 398.2 eV, which probably corresponds to the nitrogen in a nitrile form (N≡C) with a small shoulder. The main peak of the copper Cu 2p3/2 spectrum at 932.5 eV corresponds to Cu(I). The second peak at 933.3 eV potentially might suggest that there is some contribution from a copper (II), however complete absence of the shake-up satellites at higher energies characteristic of the bivalent copper allows to unambiguously rule out this possibility. This minor peak probably comes from the oxidized Cu(I)-O.

High-resolution spectra of CuSCN nanowires are shown in Figure 4 and generally follow the same trends as 2D layers. One of the important differences is the absence of the signs of oxidation on carbon, sulfur and copper spectra. Otherwise, the obtained XPS peak values are in line with the values reported for the commercial CuSCN material.[3,10,25]

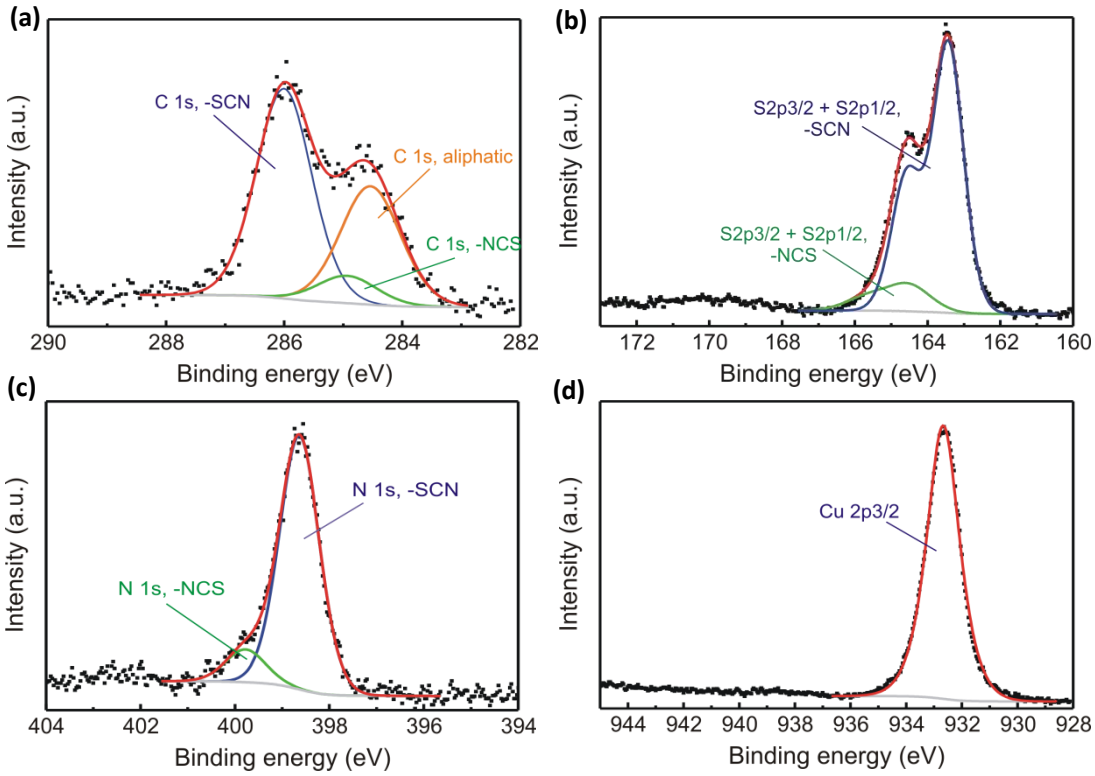

Figure 4. High-resolution XPS spectra for carbon (a), sulfur (b), nitrogen (c) and copper (d) regions for the long nanowires of CuSCN.

To perform a quantitative estimation of the composition of electrodeposited CuSCN we have removed the contributions from organic contamination (aliphatic C), and from any trace oxidized species (as seen in the C, S and Cu for 2D layers). The results of this estimation, whilst also taking into account the relative photoelectron sensitivity factors, are presented in Table 2.

Table 2. Surface elemental composition of CuSCN films determined from high-resolution XPS spectra corrected for contamination layer and oxidized species.

	Cu, %	S, %	C, %	N, %
2D layer	24.4	28.8	27.2	20.1
nanowires	25.1	27.6	28.3	19.0

The resulting elemental composition is close to the contents expected from the stoichiometry for both 2D films and nanowires with a slight deficiency of copper and nitrogen.

To gain a further insight into the origin of this slight deviation of the stoichiometry of the CuSCN films, we have performed XPS depth profiling: samples of CuSCN 2D film and nanowires on ITO were subjected to Ar^+ ion etching between the analyses. For the nanowires, the result of this profiling is shown in Figure 5 and indicates that the overestimation of carbon contents

indeed comes from a thin surface contamination layer containing adsorbed organic aliphatic molecules, which is rapidly removed after the first etch.

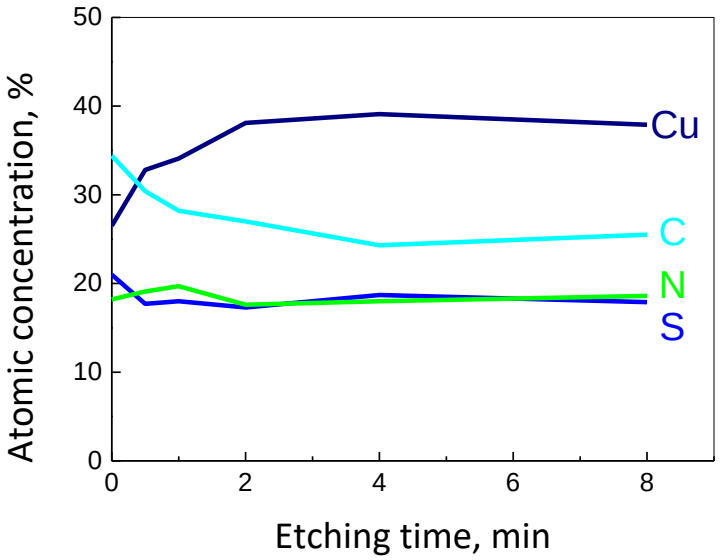

Figure 5. Depth profilometry of the atomic concentration of CuSCN nanowires obtained by etching the films by an Ar^+ ion beam. The data is not corrected for organic contamination contribution (C sp^3), which explains higher initial carbon contents as compared to table 2.

The observed initial copper deficiency is often expected to be the origin and prerequisite of good hole conductivity of CuSCN.[24] In our case after etching the copper concentration seems to increase considerably. This trend is probably just an artefact as we do not observe any additional copper containing phases, either by XRD or by XPS. The copper contents overestimation in the depth of CuSCN material is likely to occur due to a known phenomenon: in some cases during the etch the heavier elements are removed more slowly than the lighter ones, thus slightly changing the apparent concentration.[30]

While for CuSCN nanowires the composition is close to stoichiometric throughout all the samples, for the 2D films there is a slight nitrogen deficiency observable even after the etching (see Supporting information). Interestingly, a similar deficiency has already been observed in the case of electrodeposited CuSCN thin films[29] and was then explained in terms of preferential argon etching of nitrogen atoms. However, the nitrogen content in the cited reference was already lower than that expected from the stoichiometry before the etching commenced. Another hypothesis is that this observed deficiency could be related to dangling bonds or other phenomena limited to surface. Yet after the initial slight increase, the nitrogen concentration remains lower than the stoichiometric value deeper in the CuSCN material. Our

working hypothesis is that a lack of nitrogen in CuSCN 2D films could be due to partial electroreduction of the thiocyanate ion during the deposition from alkaline electrolyte.[31]

The XPS peaks of all elements - except copper - have a contribution of a second species in addition to the major peak. Very recently, similar secondary peaks found in the films fabricated from commercial CuSCN powder were explained by partial decomposition of the cyano-groups and formation of C=N bonds.[3] This explanation is not valid in our case as we do not see any characteristic signature vibrations in the Raman spectra of the C=N region (usually seen at 2070-2080 cm^{-1},[32] see figure 6 and Raman discussion), furthermore the cyano-group formation does not explain clearly visible secondary peaks of the sulfur region. We interpret this phenomenon in terms of the ambidentate character of a SCN anion, which can exist in two forms: thiocyanate ($^{-}$S-C≡N) and isothiocyanate (S=C=N^{-}).[27] The form which would dominate in a given compound depends on the nature of a corresponding cation; a thiocyanate anion is a softer base while isothiocyanate is a harder base. Copper thiocyanate in solution is a good example of its ambidentate nature. According to the Pearson acid base concept, copper (I) and (II) cations, which are a soft and an intermediate Lewis acid respectively, would be complexed in solution differently: Cu(I) is coordinated by a thiocyanate ion $[Cu(SCN)_3]^{2-}$, while Cu(II) – by isothiocyanate $[Cu(NCS)_4]^{2-}$. In addition to the hard-soft interactions, the configuration of CuSCN in a solid form also depends on the intermolecular interactions such as hydrogen bonding in solution and would thus depend on the solvent nature.[33]

Altogether, these facts have led us to the following interpretation of the peaks in the XPS spectra: the major peak corresponds to the CuSCN structure with thiocyanate bound to copper through S, while the minor peak reflects the contribution of the less energetically favourable N-bound structure. However, the logical suggestion that the N-bound compound corresponds to the copper (II) isothiocyanate $Cu(NSC)_2$ is not valid for several reasons. There are neither traces of copper (II) in the XPS spectra, nor characteristic signature vibrations in the Raman spectra of the C=N region, moreover, after the electrodeposition it is unlikely to find $Cu(NSC)_2$ in the solid form as it is soluble in water. Theoretical calculations of different CuSCN isomers predicted that both S- and N-bound thiocyanates predominantly have the ($^{-}$S-C≡N) structure, which can thus explain the absence of the characteristic signs of the isothiocyanate.[34] Based on the above, we believe that in the electrodeposited CuSCN material

two isomers coexist: Cu^{+}—$^{-}$S-C≡N and Cu^{+}—:N≡C-S^{-}. We have calculated the contribution of the minor peaks for all the elements involved and these are presented in Table 3.

Table 3. Binding energies (BE) of major and minor peaks of the XP spectra and the corresponding relative contributions of theS-bound and N-bound thiocyanate.

		S		C		N	
		S-bound	N-bound	S-bound	N-bound	S-bound	N-bound
2D layer	BE, eV	163.0	164.4	285.7	285.2	398.2	399.6
	Contents	**88.6%**	**11.4%**	**84.7%**	**15.3%**	**87.2%**	**12.8%**
Nanowires	BE, eV	163.4	163.5	286.0	284.9	398.6	399.8
	Contents	**88.0%**	**12.0%**	**87.7%**	**12.3%**	**88.5%**	**11.5%**

The composition of SCN in S- and N-bound forms roughly follows the stoichiometry and results in the predominant binding of the thiocyanate ion to the copper via the sulfur atom with approximately 12% of thiocyanate ion bound to the copper by a nitrogen atom. Moreover, in both 2D layer and nanowire form this isomer distribution remains constant.

In order to get further information on the electrodeposited CuSCN 2D thin film and nanowires we have performed Raman spectroscopy. The spectra from the samples are dominated by a series of intense sharp peaks as shown in Figure 6. In line with our previous XRD and TEM studies,[13,14] these Raman spectra provide an additional proof of high crystalline quality of the deposited CuSCN, as an amorphous material would generally show broader and less intense spectral peaks. The Raman spectroscopy is a sensitive tool to reveal any existing strain, so the similarity of the peak positions both within these samples and compared to those for the bulk CuSCN suggests that the nanowires and 2D layers are not affected by significant stress. Also, the absence of the signals at 411, 492 and 633 cm^{-1} related to the Cu-O[35] confirms the XPS observation that the electrodeposited CuSCN is not significantly oxidized to enable detection with Raman. Different thickness and transparency of the deposited samples is reflected in the amount of background signal that appears in the sample spectra with broader background behaviour appearing at 563 cm^{-1} and 1100 cm^{-1} for the thinner 2D sample and 400 nm nanowire sample.

The most intense peak at 2175 cm^{-1} seen in the spectra of figure 6 is accompanied by a satellite at 2117 cm^{-1} and likely belongs to the characteristic stretching of C≡N bonds (these have been rescaled by dividing the intensity by a factor of 7.5 to present alongside the lower wavenumber region). More precise assignment of each peak is very interesting as usually only a single peak is observed. Taking into account our hypothesis of different SCN binding modes from XPS results interpretation, and the fact that usually peaks of S-bound thiocyanate are observed at higher frequencies than N-bound one,[35,36] we assign the major peak at 2175 cm^{-1} to ν(CN) in -SCN, while the smaller one at 2117 cm^{-1} is probably due to the minor N-bound –NCS contribution already observed previously in XPS spectra. Raman spectroscopy was able to confirm the findings from XPS of the presence of two possible structures of electrodeposited CuSCN. From the figures presented in table SI-1 in the Supporting Information, we have shown the spectral contribution of both the thiocyanate bound forms. Whilst the majority of the material exists in the S- terminated thiocyanate form there is also some spectral evidence of the N- bound form (from the two peaks present in the higher wavenumber region). Further spectral evidence of N- bound thiocyanate is not observed at the lower wavenumber region where an additional vibration for (C-S) may be expected at 732 cm^{-1} for the altered configuration.[35] However, given the relative strength of the spectral response from the ν(C≡N) bond at 2175 cm^{-1} compared to that of ν(C≡N) bond at 2117 cm^{-1} for the two configurations it is likely that the relative abundance and lower cross-section of the spectral response expected for ν(C-S) would render the signal from the N- bound thiocyanate to be undetectable and thus absent in the lower wavenumber region.

The –SCN- bridging mode is commonly found in Raman spectra around 2156 cm^{-1}, but contributions to this Raman signature are not observed for any of the CuSCN samples investigated and therefore we rule out the possibility of any –SCN- bridging.

To further confirm the presence of the differently bound thiocyanates in electrodeposited films, we studied the spectra at lower frequencies in more detail. Figure 6 also shows the spectra recorded in the spectral range 100-1150 cm^{-1}, which are normalised to the maximum peak within the range (747 cm^{-1}). A rolling circle filter was also implemented to remove the background baseline without disruption to the spectral features.

The peak at 432 cm^{-1}, which corresponds to the SCN group bending, can be used as an indicator of the presence of thiocyanates predominantly in S-bound mode. The peaks of lower

intensity accompanying the major one probably come from splitting due to the low symmetry of Cu-S-CN group.[36]

A strong sharp peak at 747 cm^{-1}, which corresponds to the C-S stretching, provides further confirmation of the prevailing S-bound thiocyanate ($^{-}$S-C≡N). Finally, the wide doublet of two peaks at 203 and 244 cm^{-1} can be interpreted once again in terms of coexistence of N- and S-bound thiocyanates with the former one corresponding to Cu-S and latter to Cu-N stretching.[28,29,35]

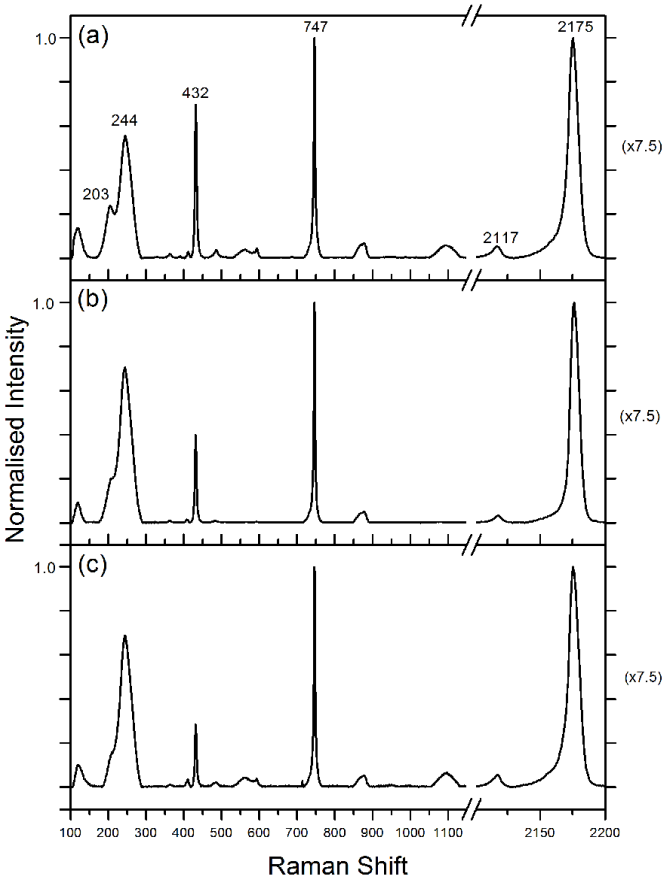

Figure 6. The mean normalised Raman spectra with baseline subtraction for the 2D platelets, 1 µm and 400 nm samples are shown in (a), (b) and (c) respectively. The spectral regions of 100-1150 cm^{-1} and 2100-2200 cm^{-1} can be seen for all samples, with the main Raman peaks of CuSCN labelled in spectrum (a). The normalised intensity in the 2100-2200 cm^{-1} wavenumber region, has been rescaled in order to plot the intense Raman response of the 2175 cm^{-1} peak on the same scale, the dividing factor of 7.5 was used and hence the right scale indicates the x7.5 factor that has to be used to interpret the higher wavenumber region.

The relative intensity of the 432 cm^{-1} peak for the 2D film was seen to be, on average, double that of the nanowire samples. This provides some possible insight into the different coordination geometry between the 2D and nanowire structures.

To further investigate the influence of the morphology of CuSCN material on its crystalline properties we have deposited by spin-coating and measured bulk CuSCN films (see Supporting information). The resulting spectrum largely corresponds to the samples of electrodeposited 2D and nanowire samples. The spin-coated bulk CuSCN sample resembles the Raman Spectra of the 2D films and nanowires. Similar asymmetric behavior is seen in the 2175 cm^{-1} peak previously assigned to the ν(C≡N) vibration of S- terminated CuSCN. The asymmetry of this peak is due to the small spectral contributions of aggregated CuSCN forms i.e. $(CuSCN)_x$.[35] There is also a small spectral contribution from the N- terminated thiocyanate as can be seen in table SI-1 (see Supporting Information). CuSCN characteristic Raman peaks in the lower wavenumber region are seen in the bulk spectrum with all the peak positions confirming β phase CuSCN[37] as seen with both the 2D films and nanowires. Spectrally, the lower wavenumber region is dominated by the convoluted metal ligand contributions of Cu-N and Cu-S. In addition the relative intensity of the 432 cm^{-1} SCN group bending peak in the bulk is stronger than that seen for either the 2D films or the nanowires. This suggests that as the structure is reduced in size the SCN bending mode is restricted and is likely related to the change in the surface to volume ratio and hence different surface coordination geometry. This was a reproducible phenomenon across multiple samples.

The question about the nature of the band gap of bulk CuSCN remains open: some studies claim that it has a direct band gap,[10] other predict that it should have an indirect one[38] and several studies interpret its band structure in terms of a direct gap with some contribution of an indirect transition.[4,25] By DFT methods it was calculated that the band gap of CuSCN is expected to be indirect, however by decreasing the copper content in the material (*i.e.* creating the copper vacancies) the band gap can become direct.[38] To the best of our knowledge no information about the band gaps of nanostructured CuSCN has been reported so far. To get a general idea about the nature of the optical band gap, a common practice is to examine the absorption coefficient (α) dependence on the energy in the Tauc plot coordinates ($(\alpha h\nu)^n$ *vs* hν). The *n* values giving rise to the most linear plot allows us to determine the nature of the band gap: if n = 2, it is considered direct; if n = 0.5, the band gap is indirect, finally for n = 2/3 we deal with a direct band gap with forbidden transition. We have plotted the absorption spectra of nanostructured CuSCN in corresponding coordinates aimed at elucidating the nature of the band gap (Figure 7). In the case of both electrodeposited

CuSCN 2D film and nanowires the Tauc plot can be fitted almost equally well with n = 2 or n = 0.5. The direct band gap value found for short nanowires equals to 3.61 eV, while the indirect transition takes place at lower energy, at 3.01 eV. For the electrodeposited 2D layer, we have recently reported the direct transition to be at about 3.80 eV,[15] while the indirect one is at 3.50 eV. Interestingly, in the case of the bulk CuSCN it was predicted from theoretical calculations that there is some kind of indirect transition situated in the gap with the energy 0.4 eV below the direct transition.[25]

This coexistence of two possible band gaps in CuSCN makes its physical interpretation complicated. If the linear regions were situated at clearly different energies, one could assume that two different energy levels were observable and thus the nature of transition with the lower energy would determine the overall nature of the band gap. In our case however, direct and indirect transitions are visible within the same energy region (3.4-4.0 eV), which could mean that they originate from different domains with slightly different gaps and become superposed on the spectrum. In a recent paper it was predicted that the nature of the band gap of CuSCN material would strongly depend on its chemical structure,[38] thus the two domains responsible for different gaps may have slight structural variation. Even though this variation should not be very pronounced as no signatures were observed by X-ray diffraction, a hint about its origin can be found in our XPS measurements, unambiguously showing the presence of two possible structures in electrodeposited CuSCN, namely N- and S-bound copper thiocyanates and this was confirmed by Raman Spectroscopy. Furthermore, most likely the domains having indirect transition largely dominate the CuSCN material as indirect gap materials have very low absorption coefficients because of the weak transition probability.

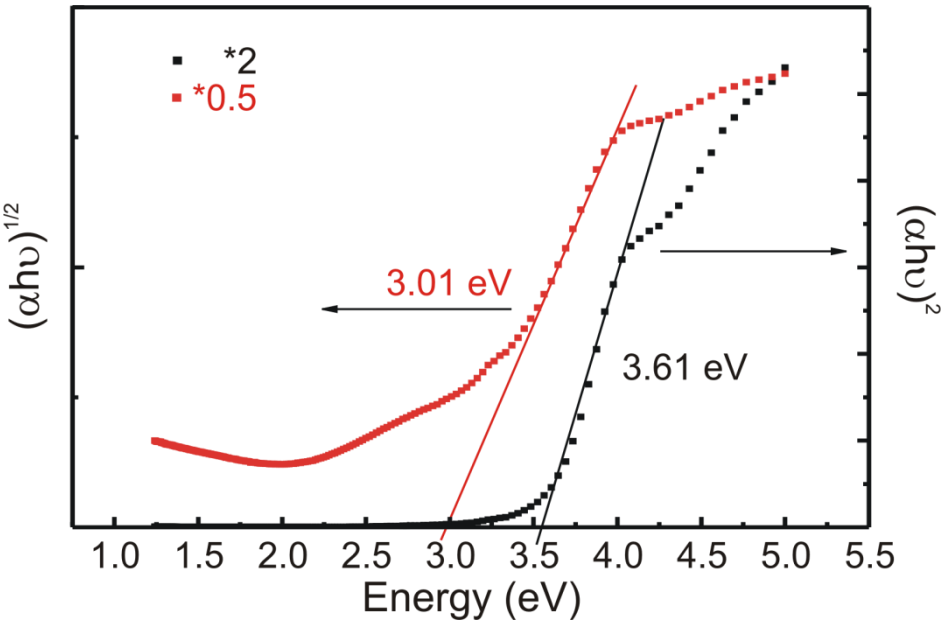

Figure 7. Tauc plots on the coordinates corresponding to direct (n=2) and indirect (n=0.5) band gap materials for CuSCN short nanowires.

Another interesting phenomenon probably related also to the unusual structure of the electrodeposited CuSCN is its strong absorption tail. Such sub-band gap absorption is often explained by the presence of transitions into the surface defects situated below the band edge and can be quantified in terms of the following relationship $\alpha \sim \exp(E/E_u)$, where α is the absorption coefficient and E_u is the Urbach energy.[39] Typically, the Urbach energy is 10-20 meV for highly organized materials, such as crystalline Si, 10-100 meV for various ligand-passivated nanocrystals[40] and up to hundreds of meV for less organised materials, such as amorphous Si or nanolayers of semiconductors deposited by SILAR or CBD methods.[41] We have determined and compared the E_u for several films by drawing the absorption spectrum in the form ln(α) *vs* E and taking the slope of the curve (Figure 8).

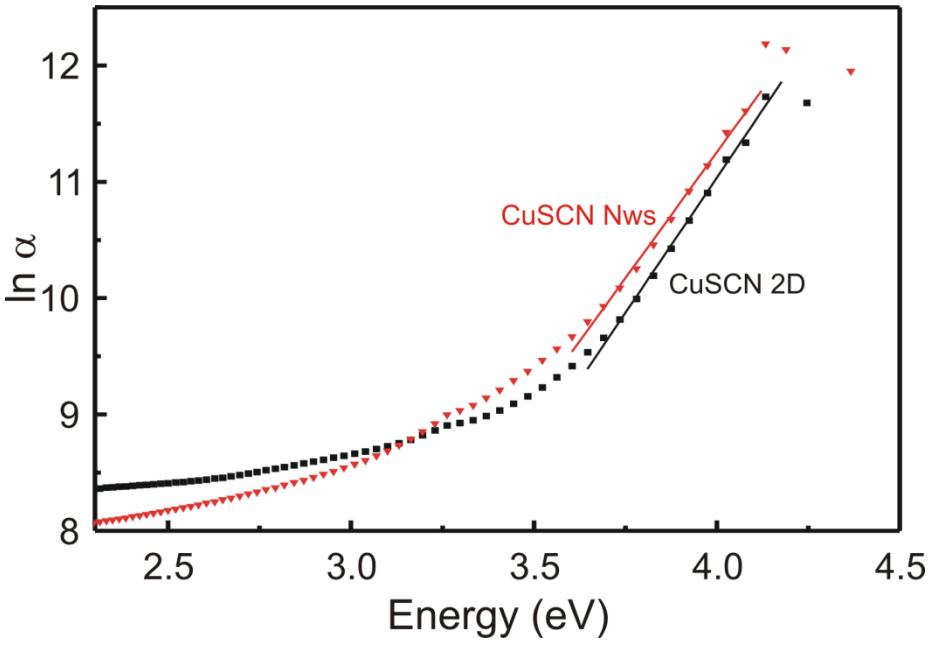

Figure 8. Urbach energy plots for CuSCN 2D (black) and short nanowires (blue)

For electrodeposited CuSCN, a material of high crystallinity, one would expect a low value of the Urbach energy, however the values of E_u were found to be 240 meV for 2D films, while for nanowires it is about 205 meV with tails extending to 1-1.5 eV beyond the band gap (*ca*. 3.8 eV). In addition, the E_u was found to be independent on nanowire length. Such relatively high Urbach energy values can be explained in terms of the presence of intragap states due to the internal strain and composition variations that might be caused by the coexistence of the two bound forms, Cu-SCN and Cu-NCS, as described in detail earlier. Moreover, the fact that these two coexisting domains have different band gap structures may provide additional explanation of unexpectedly high E_u. Another plausible explanation may come from the surface defects, such as adsorbed impurities, dangling bonds etc. For example, similar surprisingly high E_u values have been recently reported also for the hydrothermally grown ZnO nanowires (122 meV) and explained by the surface disorder after the wet chemical synthesis.[42] While Urbach energy indeed can be used as an indicator of material quality, care should be taken before directly relating it to the electronic properties. First, the concentration of possible structural or surface defects in electrodeposited CuSCN nanowires and thin films seems to be low according to Raman and XPS analysis and our previous XRD and TEM studies.[15] Second, as an example, regardless of relatively high E_u values, ZnO nanowires are known to be one of the best electron transporting materials in various electronic devices; moreover, indirectly we have already shown the excellent transport properties of various CuSCN films in

photovoltaic devices.[15] Finally, it is known that widely-studied chemically grown nanostructured metal oxides, such as ZnO and TiO_2 have a relatively high defect density immediately after the fabrication. At the same time, annealing can produce a considerable reduction in the number of these defects.[43,44] The annealing removes possible internal crystalline structure imperfections as well as passivates external surface defects, thus significantly decreasing the concentration of trap states and as a consequence improving the charge transport. Such a post-deposition treatment may also be effective at decreasing the number of defects in CuSCN and will be the subject of continued investigations on electrodeposited CuSCN nanostructures to reveal its influence on their electronic and optical properties.

Conclusions

In conclusion, using a variety of methods we have extensively characterised electrodeposited copper thiocyanate thin films and nanowires and elucidated its numerous intriguing properties explained by its unique structure. It is shown that electrodeposited CuSCN, in both 2D and nanowire forms, exhibits high crystalline quality and its composition is close to the expected stoichiometry. Interestingly, the main part of the electrodeposited β-CuSCN consists of thiocyanate bound to the copper through its S-end (Cu-S-C≡N), while 12-14% of the material exists in the N-bound form (Cu-N≡C-S). A conclusion initially drawn from the XPS analysis and corroborated by Raman spectroscopy is that the N-bound form is present as a thiocyanate, and not as an isothiocyanate (Cu-N=C=S).

The results based on the applied absorption spectroscopy (Tauc and Urbach plots) appear to be in agreement with previous studies, and show that the CuSCN material exhibits a large direct band gap combined with an indirect transition at lower energy. We assume this is a superposition of electronic signatures of two different CuSCN domains, likely to correspond to those observed by XPS and Raman. We also observe an absorption tail and high Urbach energy, which we conclude as either as a direct consequence of the particular CuSCN structure combining N- and S-bound thiocyanate domains or due to the high concentration of the trap defects. In any case, this absorption tail should not represent an obstacle for the use of the copper thiocyanate in electronic devices, particularly as the traps density is likely to be considerably reduced by annealing. At the same time, promising results have been already obtained with the non-annealed material in solar cells.[15] As a potential for further

development, we have shown that the different geometry offered by the nanowires in comparison to the 2D platelets (and both cases in relation to bulk CuSCN), appear to offer a means by which the electronic properties can be tuned and this offers exciting device opportunities for nanostructured CuSCN.

Acknowledgements. This work was supported by the *Agence Nationale de la Recherche* (ANR-13-BS10-0011-01).

Supporting Information Available. This information is available free of charge via the Internet at http://pubs.acs.org.

References

(1) Odobel, F.; Pellegrin, Y.; Gibson, E. A.; Hagfeldt, A.; Smeigh, A. L.; Hammarström, L. Recent Advances and Future Directions to Optimize the Performances of P-Type Dye-Sensitized Solar Cells. *Coord. Chem. Rev.* **2012**, *256*, 2414–2423.

(2) Thomas, S. R.; Pattanasattayavong, P.; Anthopoulos, T. D. Solution-Processable Metal Oxide Semiconductors for Thin-Film Transistor Applications. *Chem. Soc. Rev.* **2013**, *42*, 6910–6923.

(3) Pattanasattayavong, P.; Ndjawa, G. O. N.; Zhao, K.; Chou, K. W.; Yaacobi-Gross, N.; O'Regan, B. C.; Amassian, A.; Anthopoulos, T. D. Electric Field-Induced Hole Transport in copper(I) Thiocyanate (CuSCN) Thin-Films Processed from Solution at Room Temperature. *Chem. Commun.***2012**, *49*, 4154–4156.

(4) Pattanasattayavong, P.; Yaacobi-Gross, N.; Zhao, K.; Ndjawa, G. O. N.; Li, J.; Yan, F.; O'Regan, B. C.; Amassian, A.; Anthopoulos, T. D. Hole-Transporting Transistors and Circuits Based on the Transparent Inorganic Semiconductor Copper(I) Thiocyanate (CuSCN) Processed from Solution at Room Temperature. *Adv. Mater.* **2013**, *25*, 1504–1509.

(5) Gao, X.-D.; Li, X.-M.; Yu, W.-D.; Qiu, J.-J.; Gan, X.-Y. Room-Temperature Deposition of Nanocrystalline CuSCN Film by the Modified Successive Ionic Layer Adsorption and Reaction Method. *Thin Solid Films* **2008**, *517*, 554–559.

(6) Ahirrao, P. B.; Gosavi, S. R.; Sonawane, S. S.; Patil, R. S. Wide Band Gap Nanocrystalline CuSCN Thin Films Deposited by Modified Chemical Method. *Arch. Phys. Res.* **2011**, *2*, 29–33.

(7) Tennakone, K.; Kumarasinghe, A. R.; Sirimanne, P. M.; Kumara, G. R. R. A. Deposition of Thin Polycrystalline Films of Cuprous Thiocyanate on Conducting Glass and Photoelectrochemical Dye-Sensitization. *Thin Solid Films* **1995**, *261*, 307–310.

(8) O'Regan, B.; Schwartz, D. T.; Zakeeruddin, S. M.; Grätzel, M. Electrodeposited Nanocomposite N-P Heterojunctions for Solid-State Dye-Sensitized Photovoltaics. *Adv. Mater.* **2000**, *12*, 1263–1267.

(9) Selk, Y.; Yoshida, T.; Oekermann, T. Variation of the Morphology of Electrodeposited Copper Thiocyanate Films. *Thin Solid Films* **2008**, *516*, 7120–7124.

(10) Ni, Y.; Jin, Z.; Fu, Y. Electrodeposition of P-Type CuSCN Thin Films by a New Aqueous Electrolyte With Triethanolamine Chelation. *J. Am. Ceram. Soc.* **2007**, *90*, 2966–2973.

(11) Engelhardt, R.; Könenkamp, R. Electrodeposition of Compound Semiconductors in Polymer Channels of 100 Nm Diameter. *J. Appl. Phys.* **2001**, *90*, 4287–4289.

(12) Sun, L.; Ichinose, K.; Sekiya, T.; Sugiura, T.; Yoshida, T. Cathodic Electrodeposition of P-CuSCN Nanorod and Its Dye-Sensitized Photocathodic Property. *Phys. Procedia* **2011**, *14*, 12–24.

(13) Chappaz-Gillot, C.; Salazar, R.; Berson, S.; Ivanova, V. Room Temperature Template-Free Electrodeposition of CuSCN Nanowires. *Electrochem. commun.* **2012**, *24*, 1–4.

(14) Sanchez, S.; Chappaz-Gillot, C.; Salazar, R.; Muguerra, H.; Arbaoui, E.; Berson, S.; Lévy-Clément, C.; Ivanova, V. Comparative Study of ZnO and CuSCN Semiconducting Nanowire Electrodeposition on Different Substrates. *J. Solid State Electrochem.* **2012**, *17*, 391–398.

(15) Chappaz-Gillot, C.; Berson, S.; Salazar, R.; Lechêne, B.; Aldakov, D.; Delaye, V.; Guillerez, S.; Ivanova, V. Polymer Solar Cells with Electrodeposited CuSCN Nanowires as New Efficient Hole Transporting Layer. *Sol. Energy Mater. Sol. Cells* **2014**, *120*, 163–167.

(16) Hodes, G.; Cahen, D. All-Solid-State, Semiconductor-Sensitized Nanoporous Solar Cells. *Acc. Chem. Res.* **2012**, *45*, 705–713.

(17) Lévy-Clément, C.; Tena-Zaera, R.; Ryan, M. A.; Katty, A.; Hodes, G. CdSe-Sensitized P-CuSCN/Nanowire N-ZnO Heterojunctions. *Adv. Mater.* **2005**, *17*, 1512–1515.

(18) Kumara, G. R. R. A.; Konno, A.; Senadeera, G. K. R.; Jayaweera, P. V. V.; De Silva, D. B. R. A.; Tennakone, K. Dye-Sensitized Solar Cell with the Hole Collector P-CuSCN Deposited from a Solution in N-Propyl Sulphide. *Sol. Energy Mater. Sol. Cells* **2001**, *69*, 195–199.

(19) O'Regan, B. C.; Lenzmann, F. Charge Transport and Recombination in a Nanoscale Interpenetrating Network of N-Type and P-Type Semiconductors : Transient

Photocurrent and Photovoltage Studies of TiO2/Dye/CuSCN Photovoltaic Cells. *J. Phys. Chem. B* **2004**, *108*, 4342–4350.

(20) Yoshida, T.; Zhang, J.; Komatsu, D.; Sawatani, S.; Minoura, H.; Pauporté, T.; Lincot, D.; Oekermann, T.; Schlettwein, D.; Tada, H. et al. Electrodeposition of Inorganic/organic Hybrid Thin Films. *Adv. Funct. Mater.* **2009**, *19*, 17–43.

(21) Perera, V. P. S.; Pitigala, P. K. D. D. P.; Jayaweera, P. V. V.; Bandaranayake, K. M. P.; Tennakone, K. Dye-Sensitized Solid-State Photovoltaic Cells Based on Dye Multilayer−semiconductor Nanostructures. *J. Phys. Chem. B* **2003**, *107*, 13758–13761.

(22) Briscoe, J.; Gallardo, D. E.; Hatch, S.; Lesnyak, V.; Gaponik, N.; Dunn, S. Enhanced Quantum Dot Deposition on ZnO Nanorods for Photovoltaics through Layer-by-Layer Processing. *J. Mater. Chem.* **2011**, *21*, 2517–2523.

(23) Hatch, S. M.; Briscoe, J.; Dunn, S. A Self-Powered ZnO-nanorod/CuSCN UV Photodetector Exhibiting Rapid Response. *Adv. Mater.* **2013**, *25*, 867–871.

(24) Perera, V. P. S.; Senevirathna, M. K. I.; Pitigala, P. K. D. D. P.; Tennakone, K. Doping CuSCN Films for Enhancement of Conductivity: Application in Dye-Sensitized Solid-State Solar Cells. *Sol. Energy Mater. Sol. Cells* **2005**, *86*, 443–450.

(25) Jaffe, J. E.; Kaspar, T. C.; Droubay, T. C.; Varga, T.; Bowden, M. E.; Exarhos, G. J. Electronic and Defect Structures of CuSCN. *J. Phys. Chem. C* **2010**, *114*, 9111–9117.

(26) Mora-Seró, I.; Giménez, S.; Fabregat-Santiago, F.; Azaceta, E.; Tena-Zaera, R.; Bisquert, J. Modeling and Characterization of Extremely Thin Absorber (eta) Solar Cells Based on ZnO Nanowires. *Phys. Chem. Chem. Phys.* **2011**, *13*, 7162–7169.

(27) Burmeister, J. Ambidentate Ligands, the Schizophrenics of Coordination Chemistry. *Coord. Chem. Rev.* **1990**, *105*, 77–133.

(28) Luo, H.; Weaver, M. L. Surface-Enhanced Raman Scattering as a Versatile Vibrational Probe of Transition-Metal Interfaces: Thiocyanate Coordination Modes on Platinum-Group versus Coinage-Metal Electrodes. *Langmuir* **1999**, *15*, 8743–8749.

(29) Sun, L.; Huang, Y.; Anower Hossain, M.; Li, K.; Adams, S.; Wang, Q. Fabrication of TiO2⁄CuSCN Bulk Heterojunctions by Profile-Controlled Electrodeposition. *J. Electrochem. Soc.* **2012**, *159*, D323–D327.

(30) *Surface Analysis by Auger and X-Ray Photoelectron Spectroscopy*; Briggs, D.; Grant, J. T., Eds.; IM Publications, 2003.

(31) Krogulec, T.; Galus, Z. On the Electroreduction of Thiocyanates Bound to Ni(II). *J. Electroanal. Chem. Interfacial Electrochem.* **1981**, *117*, 109–118.

(32) Rannou, J.; Chabanel, M. Vibrational Study of Ionic Association in Aprotic Solvents. 8. Copper(I) Thiocyanate in Soft Donor Solvents. *Inorg. Chem.* **1985**, *24*, 2319–2320.

(33) Tchertanov, L.; Pascard, C. Statistical Analysis of Noncovalent Interactions of Anion Groups in Crystal Structures. II. Hydrogen Bonding of Thiocyanate Anions. *Acta Crystallogr. Sect. B* **1996**, *52*, 685–690.

(34) Dobado, A.; Uggla, R.; Sundberg, M. R. On the Bonding Isomerism in Three-Co-Ordinated Copper(. *J. Chem. Soc. Dalt. Trans.* **1999**, 489–496.

(35) Son, Y.; de Tacconi, N. R.; Rajeshwar, K. Photoelectrochemistry and Raman Spectroelectrochemistry of Cuprous Thiocyanate Films on Copper Electrodes in Acidic Media. *J. Electroanal. Chem.* **1993**, *345*, 135–146.

(36) Bailey, R. A.; Kozak, S. L.; Michelson, T. W.; Mills, W. N. Infrared Spectra of Complexes of the Thiocyanate and Related Ions. *Coord. Chem. Rev.* **1971**, *6*, 407–445.

(37) Bowmaker, G. A.; Hanna, J. V. IR spectroscopy of two polymorphs of copper (I) thiocyanate and of complexes of copper (I) thiocyanate with thiourea and ethylenethiourea. *Z. Naturforsch.* **2009**, *64b*, 1478-1486.

(38) Ji, W.; Yue, G.-Q.; Ke, F.-S.; Wu, S.; Zhao, H.-B.; Chen, L.-Y.; Wang, S.-Y.; Jia, Y. Electronic Structures and Optical Properties of CuSCN with Cu Vacancies. *J. Korean Phys. Soc.* **2012**, *60*, 1253–1257.

(39) Urbach, F. The Long-Wavelength Edge of Photographic Sensitivity and of the Electronic Absorption of Solids. *Phys. Rev.* **1953**, *92*, 1324.

(40) Guyot-Sionnest, P.; Lhuillier, E.; Liu, H. A Mirage Study of CdSe Colloidal Quantum Dot Films, Urbach Tail, and Surface States. *J. Chem. Phys.* **2012**, *137*, 154704–1 – 154704–154706.

(41) Rabinovich, E.; Hodes, G. Effective Bandgap Lowering of CdS Deposited by Successive Ionic Layer Adsorption and Reaction. *J. Phys. Chem. C* **2013**, *117*, 1611–1620.

(42) Zheng, K.; Žídek, K.; Abdellah, M.; Chábera, P.; Abd El-sadek, M. S.; Pullerits, T. Effect of Metal Oxide Morphology on Electron Injection from CdSe Quantum Dots to ZnO. *Appl. Phys. Lett.* **2013**, *102*, 163119.

(43) Fan, J.; Hao, Y.; Munuera, C.; Garcia-Hernandez, M.; Güell, F.; Johansson, E. M. J.; Boschloo, G.; Hagfeldt, A.; Cabot, A. Influence of the Annealing Atmosphere on the Performance of ZnO Nanowire Dye-Sensitized Solar Cells. *J. Phys. Chem. C* **2013**, *117*, 16349–16356.

(44) Djurišić, A. B.; Ng, A. M. C.; Chen, X. Y. ZnO Nanostructures for Optoelectronics: Material Properties and Device Applications. *Prog. Quantum Electron.* **2010**, *34*, 191–259.